Front. Environ. Sci. Eng. 2020, 14(3): 41
https://doi.org/10.1007/s11783-019-1218-0

RESEARCH ARTICLE

Adsorption characteristics of ciprofloxacin onto g-MoS_2 coated biochar nanocomposites

Zhenyu Yang[1], Rong Xing[1], Wenjun Zhou (✉)[1,2], Lizhong Zhu[1,2]

1 Department of Environmental Science, Zhejiang University, Hangzhou 310058, China
2 Zhejiang Provincial Key Laboratory of Organic Pollution Process and Control, Hangzhou 310058, China

HIGHLIGHTS

- The g-MoS_2 coated composites (g-MoS_2-BC) were synthesized.
- The coated g-MoS_2 greatly increased the adsorption ability of biochar.
- The synergistic effect was observed for CIP adsorption on g-MoS_2-RC700.
- The adsorption mechanisms of CIP on g-MoS_2-BC were proposed.

GRAPHIC ABSTRACT

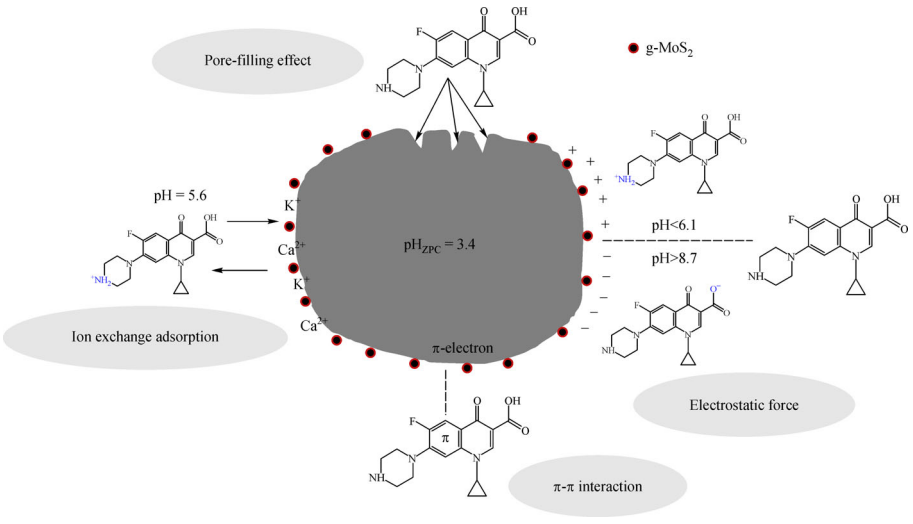

ARTICLE INFO

Article history:
Received 16 September 2019
Revised 10 December 2019
Accepted 5 January 2020
Available online 29 February 2020

Keywords:
Adsorption
Ciprofloxacin
g-MoS_2 nanosheets
Biochar
Soil remediation

ABSTRACT

The g-MoS_2 coated biochar (g-MoS_2-BC) composites were synthesized by coating original biochar with g-MoS_2 nanosheets at 300°C(BC300)/700°C (BC700). The adsorption properties of the g-MoS_2-BC composites for ciprofloxacin (CIP) were investigated with an aim to exploit its high efficiency toward soil amendment. The specific surface area and the pore structures of biochar coated g-MoS_2 nanosheets were significantly increased. The g-MoS_2-BC composites provided more π electrons, which was favorable in enhancing the π-π electron donor-acceptor (EDA) interactions between CIP and biochar. As a result, the g-MoS_2-BC composites showed faster adsorption rate and greater adsorption capacity for CIP than the original biochar. The coated g-MoS_2 nanosheets contributed more to CIP adsorption on the g-MoS_2-BC composites due to their greater CIP adsorption capacity than the original biochar. Moreover, the synergistic effect was observed for CIP adsorption on g-MoS_2-BC700, and suppression effect on g-MoS_2-BC300. In addition, the adsorption of CIP onto g-MoS_2-BC composites also exhibited strong dependence on the solution pH, since it can affect both the adsorbent surface charge and the speciation of contaminants. It was reasonably suggested that the mechanisms of CIP adsorption on g-MoS_2-BC composites involved pore-filling effects, π-π EDA interaction, electrostatic interaction, and ion exchange interaction. These results are useful for the modification of biochar in exploiting the novel amendment for contaminated soils.

1 Introduction

Antibiotics are one of the frequently detected organic pollutants and are widely used in soil treatment. Contamination of antibiotics is a global environmental problem owing to its potential threat to humans (Luo et al. 2011). Ciprofloxacin (CIP), a common fluoroquinolone antibiotic, has been used as a feed additive for animal production owing to its broad spectrum antimicrobial activities.

✉ Corresponding author
E-mail: wenjunzhou@zju.edu.cn

However, this is poorly metabolized and subsequently discharged into various environmental media such as surface water, groundwater, and farmland soil. Thus, it is extremely necessary to exploit the highly efficient soil amendments for removing antibiotic pollutants from soil, thus preventing these from entering animal and human bodies. Adsorption followed by immobilization can affect the migration/transformation of antibiotics in soil environments (Thiele-Bruhn et al. 2003), which is also regarded as a cost-effective and environmental-friendly method for the retention of antibiotics (Chen et al., 2014).

It is crucial to select suitable adsorbents to attain effective retention of antibiotics; some common adsorbents have been investigated for the adsorption/immobilization of antibiotics from soil environment, such as sediments (Wang et al., 2015), biochars (Agrafioti et al., 2014) and activated carbon. Among them, biochar showed excellent adsorption potential owing to its large specific surface area, porous structure, and abundant oxygen-containing functional groups (Cao et al., 2009; Huang et al., 2019). Compared with other adsorbents, biochar is more economical and environment-friendly, as it is originated from the pyrolysis of waste feedstock found abundantly in the environment (Ahmad et al., 2014). Recently, some modifications have been applied to enhance the adsorption capacity of biochar toward antibiotics, and these modifications includes acid treatment, metal salt activated, and nanomaterial coating (Zhao et al., 2017; Leila et al., 2014; Guo et al., 2016). Zhang et al. (2012) reported that graphene-coated biochar significantly increased the adsorption ability of target pollutants due to strengthened π-π EDA interactions between the contaminants and biochar. However, it remains challenging to develop a novel adsorbent with lower costs, eco-friendly characteristics, high adsorption efficiency, and sustainability for soil remediation.

Molybdenum disulfide (MoS_2) is a kind of layered transition metal dichalcogenide, which has a structure analogous to that of graphene. In MoS_2 crystals, the layers of Mo atoms are sandwiched between two layers of S atoms to form the S-Mo-S layered structure. Recently, some studies have shown that the S-Mo-S sandwich structure causes it to possess a huge surface area, developing pore structures and strong edge effects. Further, ultrathin MoS_2 nanosheets are used in the adsorption of antibiotics (Chao et al., 2017). Compared to graphene, g-MoS_2 nanosheets are the preferable choice for soil amendments in large scale application, as they are more abundant and cheap. However, recent adsorption studies show that g-MoS_2 nanosheets tend to agglomerate in the adsorption process, exerting detrimental influence on the adsorption/immobilization of antibiotics by g-MoS_2.

In this study, biochar was modified with g-MoS_2 nanosheets to produce the g-MoS_2-BC composites with the aim of enhancing the dispersibility of g-MoS_2 nanosheets and make best use of its preferable adsorption performance. Ciprofloxacin (CIP), the most frequently detected fluoroquinolones antibiotics in soil environment, was selected as the target contaminant, and the adsorption kinetics, adsorption efficiency, effect of pH, and adsorption mechanism of CIP on the synthesized g-MoS_2-BC composite was investigated. The main objective of the study is to elucidate the adsorption properties of g-MoS_2-BC composites for CIP and explore an effective method to exploit a novel biochar-based adsorbent in enhancing the adsorption/immobilization of antibiotics in the soil. The results of the study should provide a firm theoretical foundation for further analyses of the potential application of biochar-based composites in the adsorption of antibiotics in soil environment.

2 Materials and methods

2.1 Materials

The rice straw stocks were purchased from Jiangsu Province, China. Ciprofloxacin hydrochloride hydrate was purchased from J&K Chemical Co. Ltd. (Beijing, China). Other reagents were obtained from Aladdin Chemical Co. Ltd. (China).

2.2 Fabrication of g-MoS_2-BC composites

Biochar was obtained by pyrolyzing the rice straw samples in a preheated muffle furnace at 300°C (BC300) and 700°C (BC700) for 6 h under oxygen-deficient conditions (Cao et al., 2009). The g-MoS_2-BC composites were prepared as follows: $Na_2MoO_4 \cdot 2H_2O$ (0.03 g) thioacetamide (CH_3CSNH_2, 0.06 g) and 60 mL of deionized water were mixed together to which a certain amount of the prepared biochar was added (ratio of 20% (w/w) of MoS_2/biochar). Then, 0.1 mmol/L PEG10000 was added to disperse the mixtures. Afterwards, the solution was transferred into a 100 mL Teflonlined stainless steel autoclave; the autoclave was sealed and maintained at 180°C for 24 h. After allowing the solution to cool by itself to room temperature, the suspension was centrifuged at 8000 r/min for 15 min to collect the g-MoS_2-BC composite. The obtained mass was washed thrice with deionized water and ethanol alternatively, and dried at 80°C in air for 24 h. The g-MoS_2 nanosheets were prepared in a similar manner.

2.3 Batch adsorption experiments

Batch adsorption experiments were performed in triplicates in 22-mL tubes to determine the adsorption bebavior of CIP onto g-MoS_2-BC composites and g-MoS_2 nanosheets. An appropriate amount of the g-MoS_2-BC composites or g-MoS_2 nanosheets were mixed with 20 mL of a CIP aqueous solution. The pH of these solution was

adjusted to 5.6±0.1. The solution was equilibrated on a shaker (160 r/min) for 12 h at 25±1, followed by centrifuging it at 3500 r/min for 5 min. An appropriate amount of the supernatant was filtered through a 0.22 μm glass fiber membrane and analyzed for CIP concentrations. The adsorption amounts were calculated by considering the difference between the initial and equilibrium concentrations in aqueous solutions.

2.4 Analysis and characterization

The concentrations of CIP in aqueous solution were quantified using an Agilent 1100 HPLC (USA) fitted with an UV detector. Acetonitrile/formic acid (0.01%) (17.5: 82.5, v/v) at a flow rate of 1.0 mL/min was employed as the mobile phase for CIP, and the UV wavelength was set at 278 nm. The g-MoS_2-BC composites were characterized using a field emission scanning electron microscope (FESEM) equipped with an energy dispersive X-ray analyzer (Hitachi SU8010, Japan), Brunauer-Emmett-Teller (BET) surface analyzer (Quantachrome autosorb-1, USA), Fourier-transform infrared spectroscopy (FTIR) (Thermo FT-IRModel Nicolet 6700, USA), X-ray diffraction (XRD), X-ray photoelectron spectroscopy (XPS, ULVAC-PHI PHI 5000 VersaProbeII, Japan), and Thermogravimetric analysis (TGA) (TA-Q500, USA). The electroacoustic spectroscopy (ZS, UK) was used to measure the zeta potential of the g-MoS_2-BC composites in solution with pH in the range of 2–11.

The isotherms obtained in this study are fitted to the Freundlich and Langmuir adsorption model, respectively. The Freundlich model adsorption is determined using Eq. (1):

$$\log Q_e = \log K_F + n \log C_e, \quad (1)$$

where Q_e(mg/g) is the amount of CIP adsorbed on the adsorbents, C_e(mg/L) indicates the CIP concentration in aqueous solutions. K_F [in (mg/kg) (mg/L)$^{-n}$] and n denote the adsorption affinity and nonlinearity index, respectively.

The Langmuir equation can be described using Eq. (2):

$$C_e/Q_e = 1/(Q_{max}K_L) + C_e/Q_{max}, \quad (2)$$

where the Q_{max} (mg/g) is the maximum adsorption capacity of the adsorbents for CIP and K_L is a constant relating to the adsorption intensity.

3 Results and discussion

3.1 Characterization of the adsorbent

FESEM-Energy-dispersive X-ray spectroscopy (EDS) analysis for the BC700 and g-MoS_2-BC700 is presented in Fig. 1. It can be seen that the original biochar possessed smooth surface morphology, which was composed of closely packed tubular structures with different cavity sizes, and the surface of the g-MoS_2-BC composites was relatively uneven due to the growth of MoS_2 nanosheets on the biochar surface. It can be seen from Fig. 1b that the g-MoS_2 is an ultrathin nanosheet with numerous curved edges. The three dimensional globular-like structure of g-MoS_2-BC composites is attributed to the curling of g-MoS_2 nanosheet edges, resulting in a large surface area for the g-MoS_2-BC composites. This is significantly beneficial to the adsorption/immobilization of target contaminants.

In the EDS pattern shown in Fig. 1, we could not detect Mo in BC700, while Mo was detected in g-MoS_2-BC700, and the atomic percentage of S significantly increased from 0.54% to 9.64%; this confirms that g-MoS_2 nanosheets are coated in the prepared composites. The wide scan XPS spectra (Fig. S1) shows that the g-MoS_2-BC700 mainly consists of C, O, Mo, and S elements, and the introduction of Mo and S elements in g-MoS_2-BC composites surface is obtained by comparing the XPS spectrum of BC700 and g-MoS_2-BC700. The high-resolution XPS spectrum of Mo 3d is presented in Fig. 2(a); here, two absorption peaks at 231.9 eV and 228.5 eV are indexed to be Mo $3d_{3/2}$ and Mo $3d_{5/2}$, respectively, and this is ascribed to the Mo(+4) in 1 T-MoS_2(Xie et al., 2013). The doublet peaks located at 233.3 and 229.7 eV are assigned to the $3d_{3/2}$ and $3d_{5/2}$ of Mo^{4+} in 2H-MoS_2. The peak centered at 226.1 eV (Fig. 2(a)) can be assigned to the S_{2s} in MoS_2. The absorption peaks at 163.2 and 162.1 eV in Fig. 2(b) are the respective characteristics of S $2p_{1/2}$ and S $2p_{3/2}$ of the S_{2p} in MoS_2.

The FTIR analysis of the raw biochar and the g-MoS_2-BC composites is given in Fig. 3. It can be seen that a new stretching peak appeared at 623 cm^{-1} and is due to the γ_{as} Mo-S stretching vibration (Wang et al., 2016). This confirms presence of MoS_2 on the composite surface. In addition, the peak at 901 cm^{-1} arises from the Mo = O stretching vibration (Han et al., 2017), owing to the continual oxidation of the Mo atom on the g-MoS_2 surface.

The pore-size distribution in the original biochar and the g-MoS_2-BC composites is presented in Fig. S2. An average pore diameter of 3.251 nm is determined for the g-MoS_2-BC composites. It is well accepted that when the pore diameter of adsorbents is 1.7–3 times larger than the pollutants molecular size, the adsorption property of the adsorbents under this condition will be the finest (Tang et al., 2018). Therefore, it is reasonable to believe that the g-MoS_2-BC composites prepared in this study could be efficient for CIP adsorption based on the size of the CIP molecule.

3.2 Adsorption kinetics of CIP on g-MoS_2-BC composites

The adsorption kinetics of CIP on BC700 and g-MoS_2-BC700 is given in Fig. 4. Adsorption amount of CIP on g-MoS_2-BC700 showed a sharp increase in the first 8 h, thereafter reaching adsorption equilibrium. A relatively slower increase is observed for the CIP adsorption on

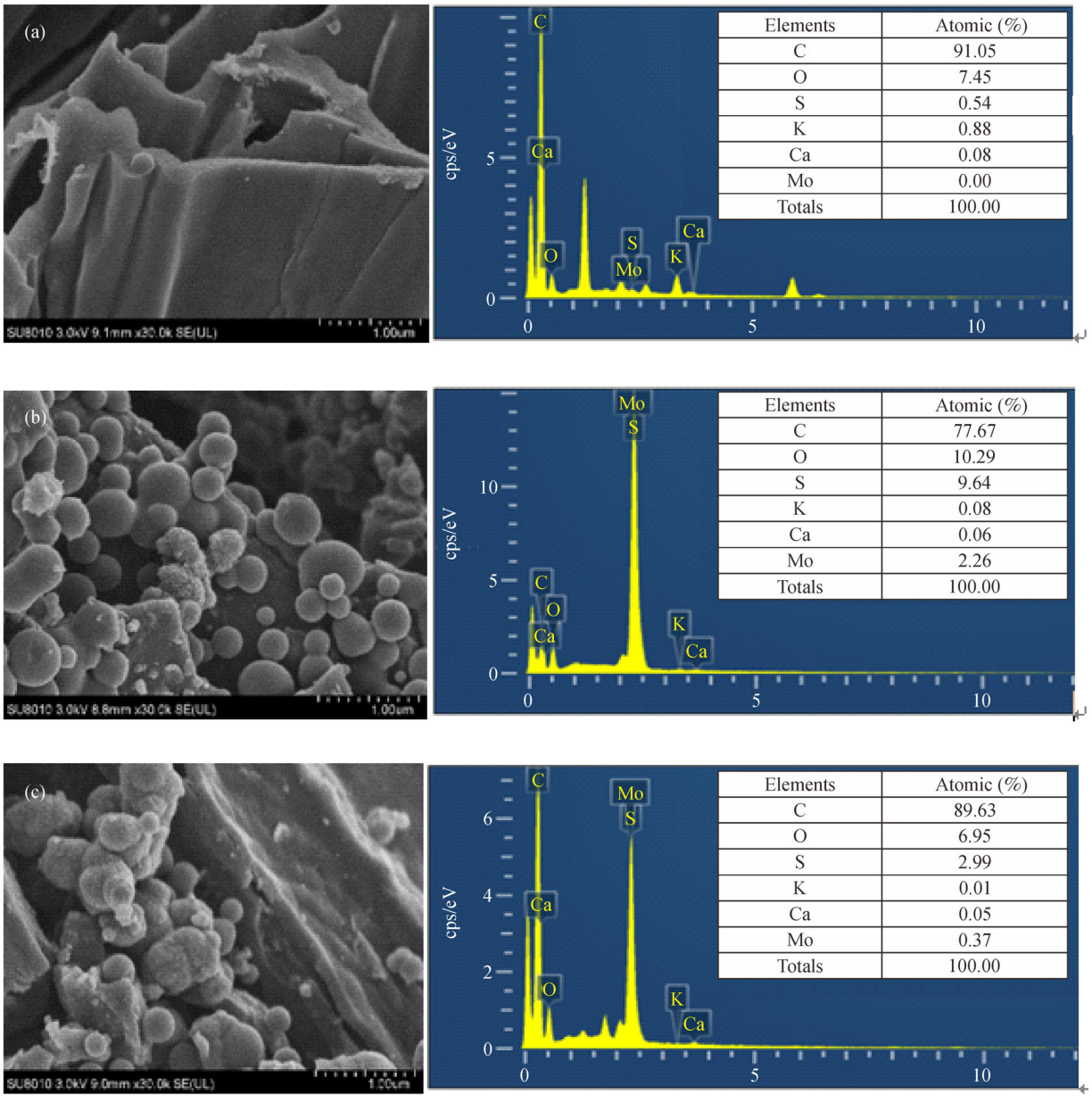

Fig. 1 SEM-EDS analyses of BC700 and g-MoS_2-BC700. (a) BC700; (b) g-MoS_2-BC700; (c) CIP loaded g-MoS_2-BC700.

BC700, and the adsorption equilibrium of CIP for is approximately 24 h. This is three times longer than for g-MoS_2-BC700. Thus, the g-MoS_2-BC composites showed faster adsorption rates for CIP than the original biochar, which can be attributed to the coating of the ultrathin nanosheets in the g-MoS_2-BC composites, and this provided more adsorption sites for CIP.

The adsorption kinetics of CIP on g-MoS_2-BC700 follows fast and slow adsorption stages. It can be seen that in the fast adsorption stage, the adsorption of CIP on g-MoS_2-BC700 sharply increased and almost 85% of the adsorption was accomplished within 4 h at all investigated concentrations, which is ascribed to accessibility of numerous adsorption sites on the adsorbent and the electrostatic attraction between g-MoS_2-BC composites and CIP. Later, the adsorption process proceeds slowly and the adsorption became almost constant after 8 h; this implies that the adsorption equilibrium has been attained.

To further analyze the kinetic characteristics of CIP adsorption on the original biochar and g-MoS_2-BC composites — the pseudo-first-order and second-order kinetic models — were used to fit the experimental adsorption data at three initial CIP concentrations, and corresponding adsorption kinetic parameters are presented in Table S1. The results showed that the pseudo-second-order model is more suitable for the adsorption behavior of

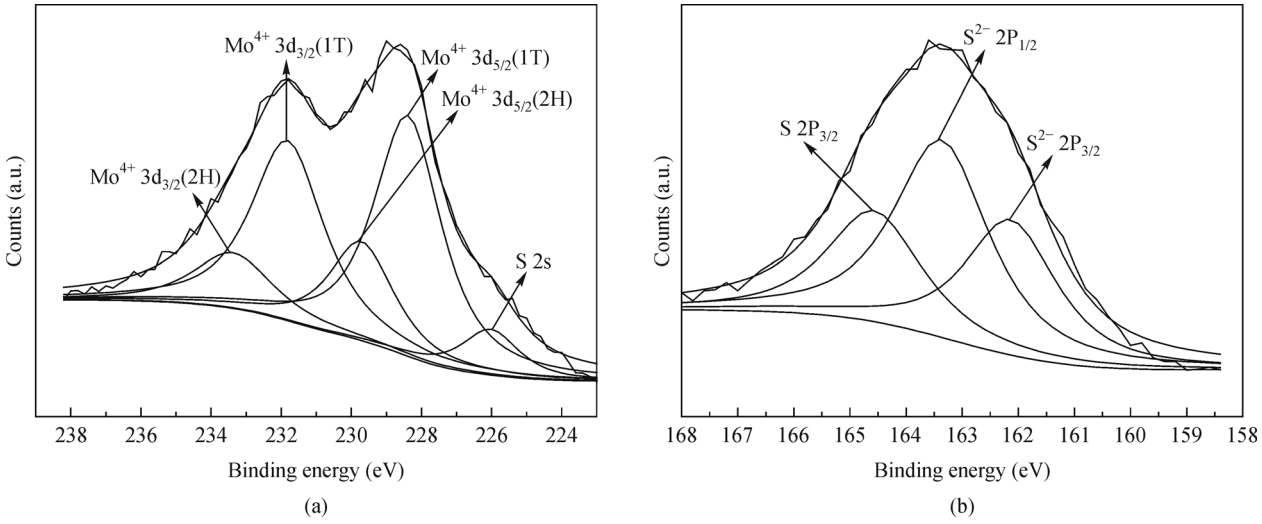

Fig. 2 The high-resolution scans of Mo 3d and S 2s (a), S 2p (b) of g-MoS_2-BC700.

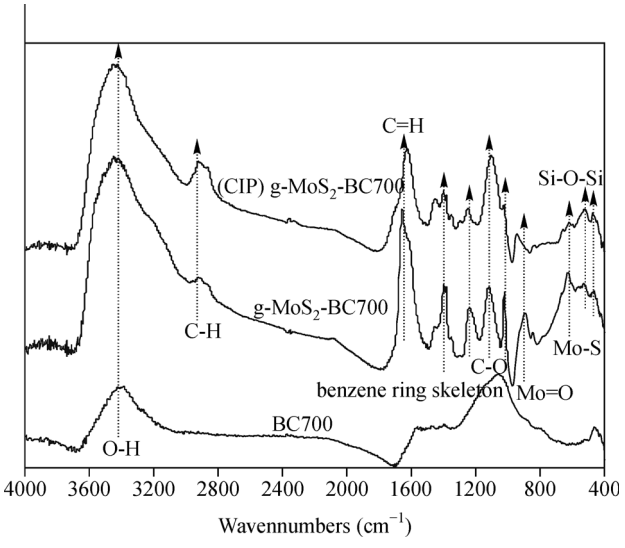

Fig. 3 FTIR spectra of BC700 and g-MoS_2-BC700.

CIP on g-MoS_2-BC composites based on the higher correlation coefficient values (R^2) in the pseudo-second-order model. This indicated that the overall rate of the adsorption process for CIP on g-MoS_2-BC composites is more likely to be controlled by chemisorption (Wang et al., 2014). Moreover, it should be noted that all k_2 and q_{max} values in the pseudo-second-order model for CIP adsorption on g-MoS_2-BC700 are much larger than that for BC700. For example, with an initial CIP concentration of 10 mg/L, the k_2 value and the corresponding q_{max} value for CIP adsorption on g-MoS_2-BC700 is about 1.4 times and 5.5 times larger than on BC700, respectively. The result shows that the adsorption ability of g-MoS_2-BC composites for CIP is significantly larger than that of the original biochar. The coated g-MoS_2 nanosheets on biochar surface adsorbed more CIP due to the presence of numerous active adsorption sites. Further, the g-MoS_2-BC composites have two-dimensional layered structures and thus, CIP was able

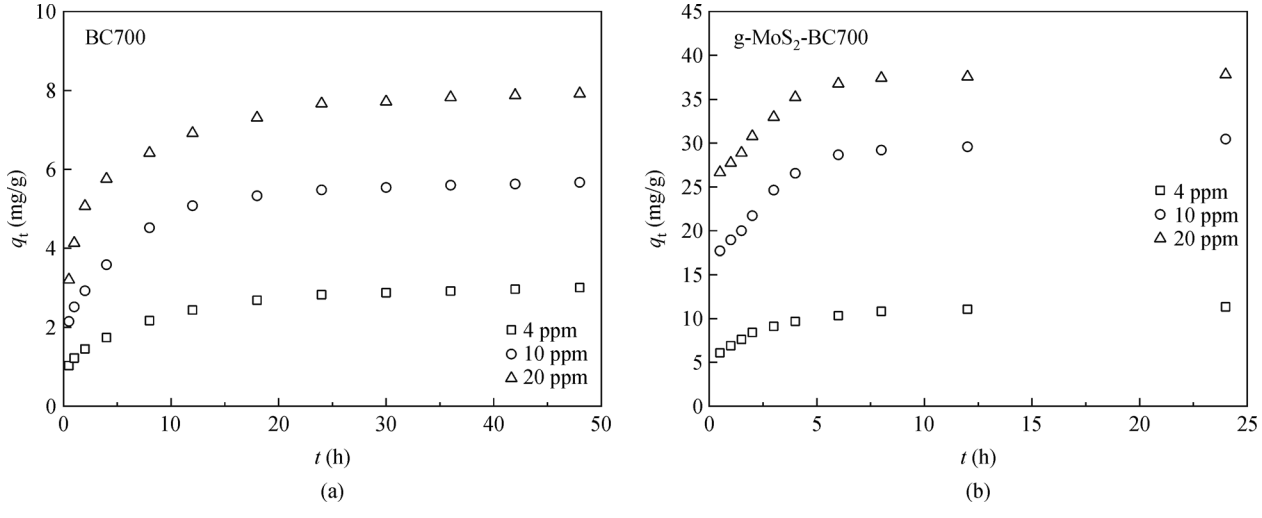

Fig. 4 Adsorption kinetics of CIP on BC700 and g-MoS_2-BC700.

to transport across the boundary liquid film from the liquid phase, whereas transport was negligible across the limited interlayer (Chao et al., 2017). This could greatly enhance the adsorption ability of CIP on g-MoS_2-BC composites.

3.3 Adsorption isotherms of CIP onto g-MoS_2-BC composites

The adsorption isotherms of CIP on original biochars, g-MoS_2 nanosheets, and the g-MoS_2-BC composites are demonstrated in Fig. 5, and adsorption data are fitted to the Freundlich model (R^2>0.99 in each case) (Table 1). It can be seen from Fig. 5 that g-MoS_2 showed greater adsorption capacity than the original biochars and g-MoS_2-BC composites. The g-MoS_2-BC composites also showed greater adsorption capacity than the corresponding original biochars and other reported biochars (Table S2). The very high surface area, developed pore structures, and strong edge effects of g-MoS_2 are responsible for the superior adsorption abilities of g-MoS_2 for CIP. To quantitatively compare the adsorption capability of the original biochar and the corresponding g-MoS_2-BC composites for CIP, the equilibrium adsorption amounts of CIP at four different initial CIP concentrations (C_0 = 4, 10, 15, and 20 mg/L) on different adsorbents are carried out and the results are listed in Table 2. For the four initial CIP concentrations, the equilibrium adsorption amount of CIP on g-MoS_2-BC700 and g-MoS_2-BC300 is about 3.9–4.9 and 3.0–3.8 times higher than that on BC700 and BC300, respectively. Therefore, the coated g-MoS_2 nanosheets greatly enhanced the adsorption ability of biochar for CIP as the adsorption capacity of g-MoS_2 for CIP is higher than the original biochars.

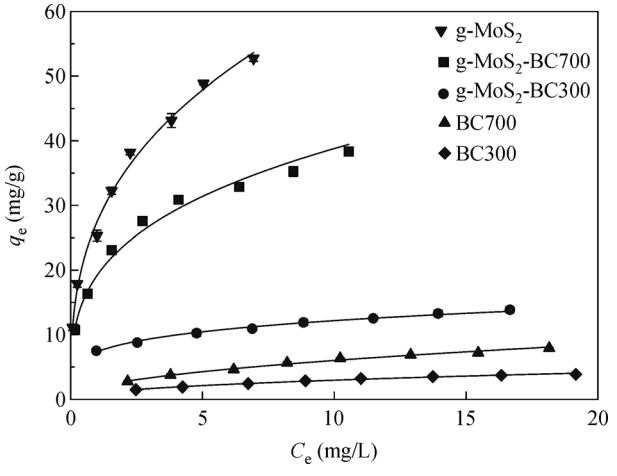

Fig. 5 Adsorption isotherms of CIP on different adsorbents.

To further explore the contribution of g-MoS_2 nanosheets and origin biochar to the overall adsorption of CIP on g-MoS_2-BC composites and the mutual effects between biochars and g-MoS_2 nanosheets, an empirical model is applied in this study (Sun et al., 2013); this is given by:

$$q_{e,cal} = \delta_{MoS_2} K_{F,MoS_2} C_e^{n,MoS_2} + \delta_{BC} K_{F,BC} C_e^{n,BC} \quad (3)$$

$$f_i = (\delta_i K_{F,i}\ C_e^{n,i}/q_{e,cal}) \times 100\% \quad (4)$$

where $q_{e,cal}$ is the theoretical adsorption amount of CIP on g-MoS_2-BC composites (mg/g) based on CIP adsorption on the g-MoS_2 nanosheets and origin biochar, respectively; BC and MoS_2 represent the mass percentage of original biochar and g-MoS_2 nanosheets in the g-MoS_2-BC composites; K_F, n are the Freundlich adsorption coefficients for CIP adsorption isotherms on g-MoS_2 and different biochars, respectively, and f_i is the percent contribution of different components for the total adsorption of CIP.

The quantitative contributions of g-MoS_2 and the original biochar to the total adsorption of CIP onto g-MoS_2-BC composites are indicated in Fig. S3. Here, C_e/S_w is the ratio of the CIP equilibrium concentration to its aqueous solubility. It is clear that the original biochar accounted only for a small percentage for CIP adsorption on the g-MoS_2-BC composites. For example, the contribution of BC300 and BC700 increased from 17.5% to 21% and from 29% to 33.2% for CIP adsorption on g-MoS_2-BC300 and g-MoS_2-BC700 with increasing CIP concentration in aqueous solutions, respectively. Meanwhile, the contribution of g-MoS_2 slightly decreased from 82.5% to 79% and from 71% to 66.8% for CIP adsorption on g-MoS_2-BC300 and g-MoS_2-BC700, respectively. The results indicate that the contribution of g-MoS_2 nanosheets for CIP adsorption on g-MoS_2-BC composites is significantly larger than that of the original biochars, and this is attributed to the huge gap of adsorption ability for CIP between them.

Moreover, the comparison between the calculated adsorption amount ($q_{e,cal}$) and experiment adsorption amount ($q_{e,exp}$) for CIP on g-MoS_2-BC composites (Fig. 6) shows a more meaningful consequence that the experimental values of $q_{e,exp}$ for CIP adsorption on g-MoS_2-BC700 at all studied CIP concentrations is larger than the calculated values of $q_{e,cal}$. However, the $q_{e,exp}$ values for CIP adsorption on g-MoS_2-BC300 is much lower than the $q_{e,cal}$ values. Therefore, the synergistic effect occurs for the CIP adsorption on g-MoS_2-BC700, but repression effect occurs on g-MoS_2-BC300. The different adsorption mechanism involved in low temperature and high temperature biochars could account for these results. It is well established that the surface adsorption and pore-filling mechanism dominate the adsorption process of organic contaminants on biochars paralyzed at high temperature (>500°C) (Xing et al., 1997), and the coated g-MoS_2 nanosheets on biochars sharply increased the surface area of biochars, which can enhance the surface pore adsorption between high temperature biochars and

Table 1 Freundlich and Langmuir model parameters for CIP adsorption on different absorbents

Sample	Freundlich model			Langmuir model		
	K_F	n	R^2	Q_{max}	K_L	R^2
BC300	0.96	0.49	0.993	4.76	0.17	0.978
g-MoS_2-BC300	7.32	0.22	0.991	12.9	1.29	0.867
BC700	1.90	0.47	0.994	9.54	0.18	0.985
g-MoS_2-BC700	19.2	0.31	0.990	37.9	2.85	0.928
g-MoS_2	27.4	0.35	0.994	39.5	0.49	0.928

Table 2 Equilibrium adsorption amount (mg/g) of CIP onto different adsorbents at four CIP initial concentrations

C_0 (mg/L)	BC300	g-MoS_2-BC300	BC700	g-MoS_2-BC700	g-MoS_2
4	1.49	7.49	2.74	10.72	11.09
10	2.85	10.92	5.62	27.58	32.25
15	3.50	12.52	6.84	32.87	43.15
20	3.85	13.85	7.89	38.33	52.75

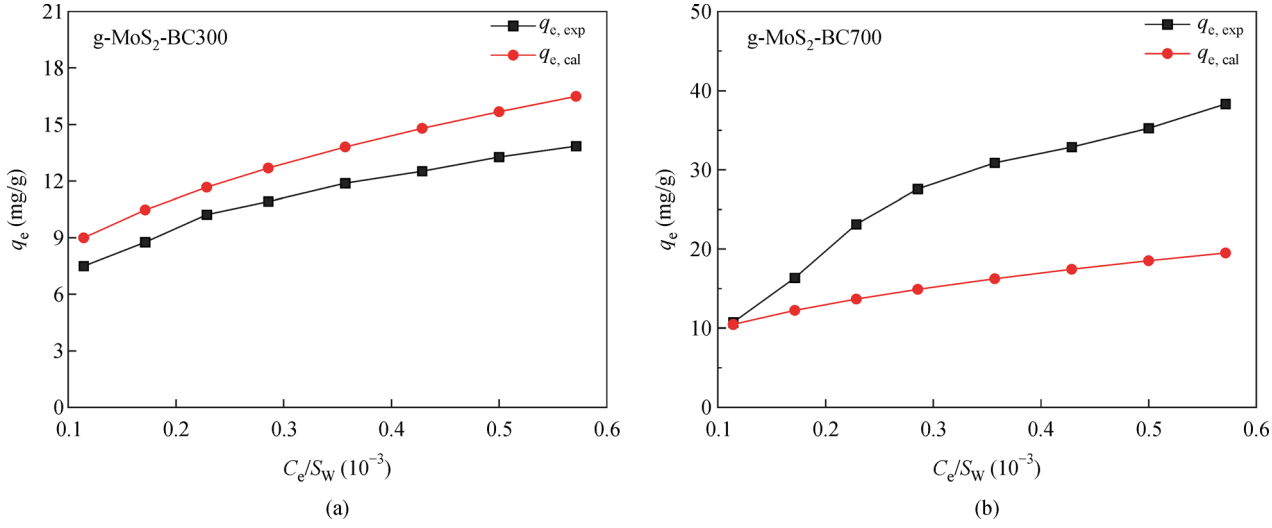

Fig. 6 Comparison of the experiment adsorption amount ($q_{e,exp}$) and the calculated adsorption amount ($q_{e,cal}$) of CIP on g-MoS_2-BC composites.

pollutants significantly. On the contrary, the surface area and pore structures of biochars paralyzed at low temperature are limited. Low temperature biochars are rich in oxygen-containing functional groups, such as C-O and C = O, which can result in negatively charged biochar due to deprotonation. The electrostatic interactions between negatively charged biochar and CIP^+ (at tested pH, CIP existed mainly as CIP^+) may be considered as the primary reason for the CIP adsorption on biochars paralyzed at low temperature.

3.4 Effect of pH on CIP adsorption on g-MoS_2-BC composites

It was well known that the solution pH plays an important role in the adsorption process owing to its effect on both adsorbent and pollutant properties. The influence of the pH of the solution on CIP adsorption on g-MoS_2-BC composites is investigated with initial CIP concentration of 10 mg/L and pH varying from 2 to 11. The result is presented in Fig. 7, which also shows the zeta potentials of g-MoS_2-BC700. The results showed that the adsorption amount of CIP increased by 34% from 21.5 mg/g to 28.8 mg/g with the pH increase from 2 to 6. However, slight change is observed with the pH value ranging from 6 to 8; then, CIP adsorption amount reduced by 41% from 28.8 mg/g to 16.9 mg/g with pH increase from 8 to 11. The result is different from the previous studies (Shang et al., 2016), where the adsorption capacity of biochar for CIP increased with pH increase from 3 to 7 and decreased with pH increase from 7 to 10. They attributed that the functional groups on the surface of biochar changed with the pH. Further, the different surface charge of the adsorbents might be responsible for the different results.

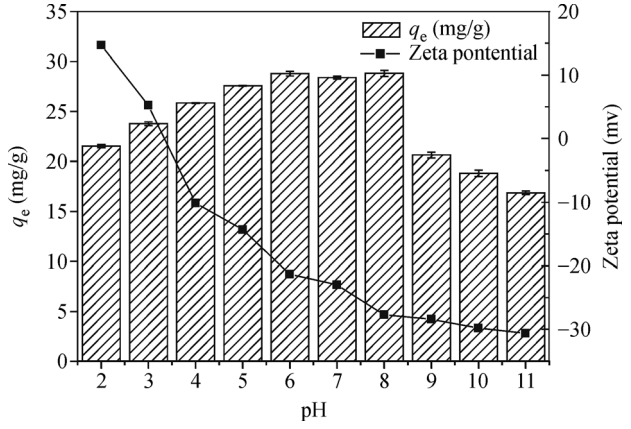

Fig. 7 Effect of solution pH on the adsorption of CIP on g-MoS_2-BC700.

The surface charge of g-MoS_2-BC composites is closely related to the solution pH value. Results from Fig. 7 showed that the pH_{ZPC} of g-MoS_2-BC700 is approximately 3.4, and g-MoS_2-BC700 is negatively charged and reduces with increase of pH when the pH>pH_{ZPC}. The transformation of protonation and de-protonation by oxygen-containing functional groups at different pH can alter the adsorbent surface charge and affect the speciation existence of organic contaminants (Tan et al., 2016). CIP is an amphoteric molecule with some ionizable functional groups, such as-NH and-COOH, which can exist as cations (CIP^+), zwitterions ($CIP^{\pm}$), and anions(CIP^-) under different pH solutions. CIP existed as CIP^+ at solution pH below 3.4, and the g-MoS_2-BC700 surface under such condition is positively charged and decreases with increasing solution pH. This indicates that the decrease of electrostatic repulsion between g-MoS_2-BC700 and CIP, will be useful for CIP adsorption. CIP mainly existed as $CIP^{\pm}$ in the pH range of 6 to 8; as a result, there is nearly no net electrostatic attraction or repulsion between CIP and g-MoS_2-BC700. Thus, the effect of pH on CIP adsorption onto g-MoS_2-BC700 under such pH range is slight. The adsorption capacity of CIP under this pH range can be controlled by other mechanisms, such as surface adsorption, π-π EDA interactions (Chao et al., 2017), which will be discussed later. CIP mainly existed in the form of CIP^- when the solution pH ranged from 9 to 11. The surface of g-MoS_2-BC700 is also negative charged in this pH range and thus, the electrostatic repulsion between g-MoS_2-BC700 and CIP^- is enhanced, which results in the reduction of CIP adsorption on g-MoS_2-BC700.

3.5 Adsorption mechanisms of CIP on g-MoS_2-BC composites

Based on the above analysis, it is reasonable to believe that various different mechanisms are involved in CIP adsorption on g-MoS_2-BC composites, which is presented in Fig. 8. The above description about the effect of solution pH on CIP adsorption onto g-MoS_2-BC composites

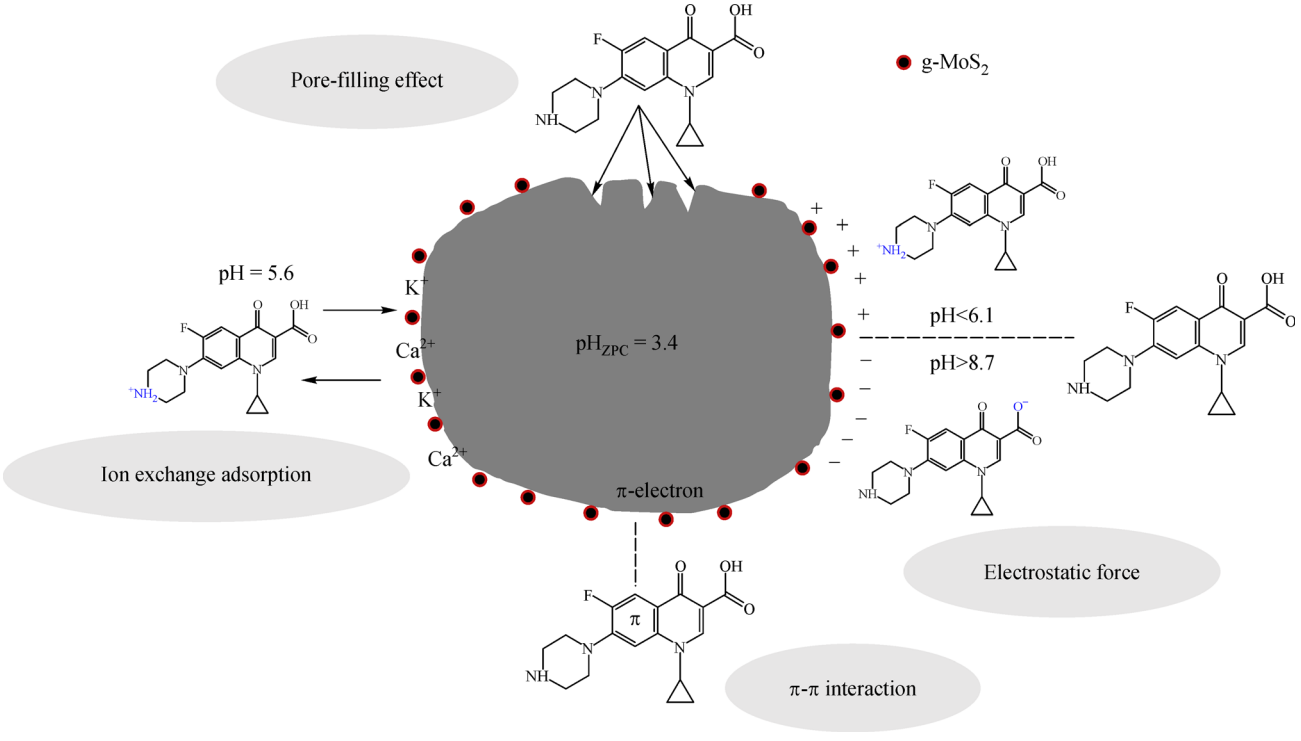

Fig. 8 The proposed adsorption mechanisms for CIP on g-MoS_2-BC composites.

confirms that the electrostatic interactions between g-MoS_2-BC composites and CIP actually exists. The FTIR spectrum (Fig. 3) for g-MoS_2-BC700 before and after CIP adsorption is further analyzed to investigate the different adsorption mechanisms of CIP on g-MoS_2-BC composites. It is known that the carboxyl group of adsorbents can cause the adsorbent surface to become negatively charged owing to its ionization. The absorption peaks at 1022 cm^{-1}, 1118 cm^{-1}, and 1241 cm^{-1} show that the C-O stretching vibration shifted to 1028 cm^{-1}, 1104 cm^{-1}, and 1249 cm^{-1}, respectively, and the C = O stretching vibration at 1657 cm^{-1} changed to 1625 cm^{-1} after the CIP adsorption. This could be ascribed to deprotonation of the carboxyl group. The result confirms the electrostatic forces between CIP and g-MoS_2-BC composites in the adsorption of CIP. Furthermore, the stretching peak at 1396 cm^{-1} derived from the aromatic benzene ring skeleton in g-MoS_2-BC700 shifted to 1402 cm^{-1} after CIP adsorption, suggesting that the π-π EDA effect between benzene ring of g-MoS_2-BC composites and other functional groups of CIP molecule is involved in CIP adsorption onto g-MoS_2-BC composites. In fact, CIP possessed a fluorine group bonded to the benzene ring and can serve as the π electron acceptor (Yang et al. 2012), while the hydroxyl group on adsorbents surface can serve as π electron donors (Han et al. 2016). Thus, it is reasonable to believe that the π-π EDA interactions between the fluorine group of CIP molecule and the hydroxyl group on g-MoS_2-BC composites surface is involved in CIP adsorption. It should also be noted that the coated g-MoS_2 nanosheets significantly increased the-OH content on g-MoS_2-BC composites (Fig. 3), resulting in π-π EDA interactions between g-MoS_2-BC composites and CIP and is much greater than on the original biochars thereby, significantly increasing the adsorption of CIP on g-MoS_2-BC composites.

Pore size distribution in g-MoS_2-BC700 during CIP adsorption is presented in Fig. S2. The composite is mesoporous, and the pore size ranged from 2 to 16 nm. However, the pore size sharply reduced after CIP adsorption, indicating that the pore-filling effect is the important mechanism of CIP adsorption on g-MoS_2-BC composites. The average pore diameter and the specific surface area (SSA value) of the g-MoS_2-BC700 and BC700 are calculated to be 3.251 nm, 7.763 nm, and 610.4 m^2/g, 140.1 m^2/g, respectively. The g-MoS_2 coated nanosheets greatly changed the pore structures and surface area of biochar and thus, an enhanced surface pore adsorption between biochar and pollutant is favored, which could significantly increase CIP adsorption on g-MoS_2-BC composites. Moreover, the EDS spectrum of g-MoS_2-BC700 before and after CIP adsorption (Fig. 1) shows that the atomic percentage of K and Ca reduced from 0.08% and 0.06% to 0.01% and 0.05%, respectively. This indicates that the ion exchange adsorption of CIP^+ with K^+ and Ca^{2+} has a key role in CIP adsorption on g-MoS_2-BC composites.

4 Conclusions

We report a novel method to synthesize g-MoS_2-BC composites by coating g-MoS_2 nanosheets into original biochar. The prepared g-MoS_2-BC composites showed excellent performance for CIP adsorption due to its appropriate pore structure and abundant π electrons. The adsorption mechanism of CIP on g-MoS_2-BC composites is attributed to the pore-filling effects, π-π EDA interactions, electrostatic interactions, and ion exchange adsorption. We also found that the adsorption strongly depends on the pH of the solution. The composites synthesized in this study are versatile and low cost and thus, they are effective materials for antibiotic immobilization from contaminated soils.

Acknowledgements This work was supported by the National Key Research and Development Program of China (No. 2018YFC1800704) and the National Natural Science Foundation of China (No. 21577124).

Electronic Supplementary Material Supplementary material is available in the online version of this article at https://doi.org/10.1007/s11783-019-1218-0 and is accessible for authorized users.

References

Agrafioti E, Kalderis D, Diamadopoulos E (2014). Arsenic and chromium removal from water using biochars derived from rice husk, organic solid wastes and sewage sludge. Journal of Environmental Management, 133: 309–314

Ahmad M, Rajapaksha A U, Lim J E, Zhang M, Bolan N, Mohan D, Vithanage M, Lee S S, Ok Y S (2014). Biochar as a sorbent for contaminant management in soil and water: A review. Chemosphere, 99: 19–33

Cao X D, Ma L N, Gao B, Harris W (2009). Dairy-manure derived biochar effectively sorbs lead and atrazine. Environmental Science & Technology, 43(9): 3285–3291

Chao Y, Yang L, Ji H, Zhu W, Pang J, Han C, Li H (2017). Graphene-analogue molybdenum disulfide for adsorptive removal of tetracycline from aqueous solution: equilibrium, kinetic, and thermodynamic studies. Environmental Progress & Sustainable Energy, 36(3): 815–821

Chen C P, Zhou W J, Yang Q, Zhu L F, Zhu L Z (2014). Sorption characteristics of nitrosodiphenylamine (NDPhA) and diphenylamine (DPhA) onto organo bentonite from aqueous solution. Chemical Engineering Journal, 240: 487–493

Guo XT, Dong H, Yang C, Zhang Q, Liao CJ, Zha FG, Gao LM (2016). Application of goethite modified biochar for tylosin removal from aqueous solution. Colloid surface A, 502:81–88

HanL, Ro K S, Sun K, Sun H, Wang Z, Libra J A, Xing B. (2016). New evidence for high sorption capacity of hydrochar for hydrophobic organic pollutants. Environmental Science & Technology, 50(24): 13274–13282

Han S, Liu K, Hu L F, Teng F, Yu P P, Zhu Y F (2017). Superior adsorption and regenerable dye adsorbent based on flower-like molybdenum disulfide nanostructure. Scientific Reports, 7(10):

43599

Huang Q, Song S, Chen Z, Hu B, Chen J, Wang X (2019). Biochar-based materials and their applications in removal of organic contaminants from wastewater: State-of-the-art review. Biochar, 1(1): 45–73

Karimnezhad L, Haghighi M, FatehifarE(2014). Adsorption of benzene and toluene from waste gas using activated carbon activated by $ZnCl_2$. Frontiers of Environmental Science & Engineering, 8(6): 835–844

Luo Y, Xu L, Rysz M, Wang Y, Zhang H, Alvarez P J J (2011). Occurrence and transport of tetracycline, sulfonamide, quinolone, and macrolide antibiotics in the Haihe River Basin, China. Environmental Science & Technology, 45(5): 1827–1833

Shang J G, Kong X R, He L L, Li W H, Liao Q J H (2016). Low-cost biochar derived from herbal residue: Characterization and application for ciprofloxacin adsorption. International Journal of Environmental Science and Technology, 13(10): 2449–2458

Sun K, Ran Y, Yang Y, Xing B S, Mao J (2013). Interaction mechanism of benzene and phenanthrene in condensed organic matter: Importance of adsorption (nanopore-filling). Geoderma, 204–205: 68–74

Tan X, Liu S, Liu Y, Gu Y, Zeng G, Cai X, Yan Z, Yang C, Hu X, Chen B (2016). One pot synthesis of carbon supported calcined-Mg/Al layered double hydroxides for antibiotic removal by slow pyrolysis of biomass waste. Scientific Reports, 6(12): 39691

Tang L, Yu J F, Pang Y, Zeng G M, Deng Y C, Wang J J, Ren X Y, Ye S J, Peng B, Feng H P (2018). Sustainable efficient adsorbent: Alkali-acid modified magnetic biochar derived from sewage sludge for aqueous organic contaminant removal. Chemical Engineering Journal, 336: 160–169

Thiele-Bruhn S, SÊren TB (2003). Pharmaceutical antibiotic compounds in soil: A review. Journal of Plant Nutrition and Soil Science, 166(2): 145–167

Wang H, Wen F, Chen Y, Sun T, Meng Y, Zhang Y (2016). Electrocatalytic determination of nitrite based on straw cellulose/molybdenum sulfide nanocomposite. Biosensors & Bioelectronics, 85: 692–697

Wang J, Wang C, Huang Q, Ding F, He X (2015). Adsorption of PAHs on the sediments from the yellow river delta as a function of particle size and salinity. Soil & Sediment Contaminant, 24(2): 103–115

Wang R, Cai X, Shen F (2014). TiO_2 hollow microspheres with mesoporous surface: Superior adsorption performance for dye removal. Applied Surface Science, 305: 352–358

Xie J F, Zhang J J, Li S, Grote F B, Zhang X D, Zhang H R, Wang X, Lei Y, Pan B C, Xie Y (2013). Controllable disorder engineering in oxygen-incorporated MoS_2 ultrathin nanosheets for efficient hydrogen evolution. Journal of the American Chemical Society, 135(47): 17881–17888

Xing B, Pignatello J J (1997). Dual-mode sorption of low-polarity compounds in glassy poly (Vinyl Chloride) and soil organic matter. Environmental Science & Technology, 31(3): 792–799

Yang W, Lu Y, Zheng F, Xue X, Li N, Liu D (2012). Adsorption behavior and mechanisms of norfloxacin onto porous resins and carbon nanotube. Chemical Engineering Journal, 179: 112–118

Zhang M, Gao B, Yao Y, Xue Y, Inyang M (2012). Synthesis, characterization, and environmental implications of graphene-coated biochar. Science of the Total Environment, 435–436: 567–572

Zhao N, Zhao C F, Lv Y Z, Zhang W F, Du Y G, Hao Z P, Zhang J (2017). Adsorption and coadsorption mechanisms of Cr(VI) and organic contaminants on H_3PO_4 treated biochar. Chemosphere, 186: 422–429